

## Prompt fission product yields in the $^{238}\text{U}(\text{n},\text{f})$ reaction

N. Fotiades, P. Casoli, P. Jaffke, M. Devlin, O. Nelson R, T. Granier, P. Talou, T. Ethvignot

► **To cite this version:**

N. Fotiades, P. Casoli, P. Jaffke, M. Devlin, O. Nelson R, et al.. Prompt fission product yields in the  $^{238}\text{U}(\text{n},\text{f})$  reaction. *Physical Review C*, American Physical Society, 2019, 99, pp.024606. cea-02339675

**HAL Id: cea-02339675**

**<https://hal-cea.archives-ouvertes.fr/cea-02339675>**

Submitted on 4 Nov 2019

**HAL** is a multi-disciplinary open access archive for the deposit and dissemination of scientific research documents, whether they are published or not. The documents may come from teaching and research institutions in France or abroad, or from public or private research centers.

L'archive ouverte pluridisciplinaire **HAL**, est destinée au dépôt et à la diffusion de documents scientifiques de niveau recherche, publiés ou non, émanant des établissements d'enseignement et de recherche français ou étrangers, des laboratoires publics ou privés.

# Yields $Y(Z, A)$ for selected $(Z, A)$ s in the $^{238}\text{U}(n, f)$ reaction

N. Fotiades<sup>1,\*</sup>, P. Casoli<sup>2</sup>, P. Jaffke<sup>3</sup>, M. Devlin<sup>1</sup>,  
R. O. Nelson<sup>1</sup>, T. Granier<sup>4</sup>, P. Talou<sup>3</sup>, and T. Ethvignot<sup>5</sup>

<sup>1</sup>*Physics Division, Los Alamos National Laboratory,  
Los Alamos, New Mexico 87545, USA*

<sup>2</sup>*Den-SERMA, CEA, Université Paris-Saclay, F-91191, Gif-sur-Yvette, France*

<sup>3</sup>*Theoretical Division, Los Alamos National Laboratory,  
Los Alamos, New Mexico 87545, USA*

<sup>4</sup>*Autorité de Sûreté Nucléaire, 92120, Montrouge, France*

<sup>5</sup> *CEA, DAM, DIF, F-91297 Arpajon, France*

(Dated: March 26, 2018)

## Abstract

**Background:** Significant yield discrepancies (500-600%) were reported recently between experimental results and predictions (from the GEF model) and evaluations (from the JEFF-3.1.1 and ENDF/B-VII.1 libraries) for Mo and Sn fission-fragment yields in fast-neutron induced reactions on  $^{238}\text{U}$  using  $\gamma$ - $\gamma$ - $\gamma$  coincidence spectroscopy. The model/evaluations also predict Mo and Sn fragments that are on average  $\sim 1$  to 2 neutrons richer than the experimental results.

**Purpose:**  $\gamma$ - $\gamma$ - $\gamma$  coincidence spectroscopy favors detection of higher-multiplicity  $\gamma$ -ray cascades. An alternative approach is determining the fragment yields using single- $\gamma$ -ray spectroscopy, as it was attempted here for selected cases where it was feasible. Advantages/drawbacks in both approaches need to be understood and potential systematic errors in the experimental results should be addressed using theoretical models.

**Methods:** Fast neutrons from the LANSCE/WNR facility were used to induce fission on  $^{238}\text{U}$  to determine the yield of selected even-even fission fragments. The selection was based on the ability to reliably determine excitation functions for the detected  $\gamma$  rays.

**Conclusions:** Our single- $\gamma$ -ray results provide better agreement between experiment and predictions/evaluations.

---

\*fotia@lanl.gov

## I. INTRODUCTION

Gamma-ray spectroscopic studies of fission fragments have been made since the seventies [1]. Detailed results were reported for spontaneous fission of actinides [2, 3] and in fission of compound nuclei formed in fusion-evaporation reactions [4, 5]. Such studies are usually limited to even- $Z$ -even- $A$  fission fragments because in all other cases the level schemes are fragmented and the  $\gamma$ -ray decay paths to the ground states are much more complicated making it difficult to perform a reliable intensity sum.

For fast neutron-induced reactions on actinides, an early study in the fission of  $^{238}\text{U}$  with  $E_n = 1.5\text{-}3.5$  MeV [6] was limited to even- $A$  Zr, Te, Xe, and Ba fragments only. Fission fragment yields in  $^{238}\text{U}(n, f)$  reactions also have been attempted using radiochemical techniques to separate the isotopes [7, 8] and using X-ray spectroscopy [9].

Recently, a more extensive study in Ref. [10] reported significant yield discrepancies between experimental results and theoretical predictions and evaluations for the even- $A$  Mo/Sn complementary fragments in  $^{238}\text{U}(n, f)$  reactions with  $E_n = 0.7\text{-}3.0$  MeV (mean energy 1.72 MeV, and a spread at half-maximum of approximately 1 MeV). The predictions are reported to overestimate the experimental Mo/Sn yields by 500-600% and the position of the average yields, for a given charge, by 1 to 2 neutrons. The Mo/Sn fragment pair is associated with the “standard-1” ( $S1$ ) fission mode and, thus, an overestimation by the prediction of the importance of spherical shell effects at scission is implied. These discrepancies were studied further in the present work using single- $\gamma$ -ray spectroscopy.

## II. EXPERIMENT

The  $\gamma$  rays produced in the bombardment of the  $^{238}\text{U}$  target by neutrons were measured with the GEANIE spectrometer [11]. GEANIE was located 20.34 m from the Los Alamos Neutron Science Center’s Weapons Neutron Research (LANSCE-WNR) facility’s spallation neutron source [12, 13] on the 60R (60°-Right) flight path. The neutrons were produced in a  $^{nat}\text{W}$  spallation target driven by an 800 MeV proton beam. The beam time structure consisted of 725  $\mu\text{s}$ -long “macropulses” at 40 Hz rate. Each macropulse contained approximately 416 “micropulses” spaced every 1.8  $\mu\text{s}$ . The energy of the neutrons was determined using the time-of-flight technique. GEANIE was comprised of 11 Compton-suppressed planar Ge

detectors (low-energy photon spectrometers, or LEPS), 9 Compton suppressed coaxial Ge detectors, and 6 unsuppressed coaxial Ge detectors.

The  $^{238}\text{U}$  target consisted of two foils, 840 mg/cm<sup>2</sup> thick in total. The foils were 99.8% enriched in  $^{238}\text{U}$ , the rest being mostly  $^{235}\text{U}$  and very little  $^{234}\text{U}$ . Four natural Fe foils, 165 mg/cm<sup>2</sup> thick in total, were placed two in front and two in back of the  $^{238}\text{U}$  foils so that the cross section of the strong 846.8-keV line of  $^{56}\text{Fe}$  from inelastic scattering [14] could be used as a check on the cross sections obtained. The target was rotated to 109° about the vertical with respect to the neutron beam.

A schematic diagram of the experimental setup can be found in Ref. [15] where the results on the  $^{238}\text{U}(n, xn\gamma)$  partial  $\gamma$ -ray cross sections from this experiment were reported. Partial results pertaining to fission fragments from this experiment were previously published in Ref. [16, 17], while the complete analysis and results on fission fragments were described in a Ph. D. thesis in Ref. [18].

### III. EXPERIMENTAL RESULTS

Partial  $\gamma$ -ray cross sections were obtained for 23 previously known transitions [19–34] of 18 fragments of Kr, Sr, Zr, Mo, Sn, Te, Xe, Ba, and Ce. The cross sections are listed in Table I for the induced-neutron energy bin of  $E_n = 1.5\text{--}2.0$  MeV (mean energy 1.75 MeV comparable to the mean energy used in Ref. [10]). In the same experiment, data were obtained for higher induced-neutron energies and are described elsewhere [16–18].

The excitation functions for all transitions in Table I follow the general shape of the  $^{238}\text{U}(n, f)$  cross section with a threshold at  $E_n \sim 1$  MeV and a second-chance fission threshold at  $E_n \sim 6$  MeV, hence, they are, most likely, emitted only by fission fragments, without any cross-section contribution from the  $^{238}\text{U}(n, xn\gamma)$  transitions reported in Ref. [15]. As an example, the cross sections obtained for two transitions in Table I are shown in Fig. 1 and are compared with the shape of the total  $^{238}\text{U}(n, f)$  cross section in the ENDF/B-VII.1 library [35]. Excitation functions determined for GEANIE-observed transitions have been regularly used to assign transitions to specific isotopes. This has been proven especially useful in assigning previously unknown transitions to  $(n, xn)$  ( $x = 1 - 7$ ) reaction-channel isotopes, (see, for instance, Refs. [36–38]). In the present work this method is used only for previously known  $\gamma$  rays that are emitted from fission fragments. The different excitation-

function shapes obtained for transitions emitted in  $(n, xn)$  reaction channels and in fission provides a rather robust criterion that can be used to differentiate between these reaction mechanisms.

Lack of experimental results for some fragments is mostly due to two or more  $\gamma$  rays forming inseparable peaks in the spectra at about the same incident-neutron energies, hence, the contribution of each  $\gamma$  ray could not be deduced. For instance, the cross section for the 151.8 keV transition of  $^{102}\text{Zr}$  in Table I includes also contributions from two previously-known yrast 152.1 keV transitions of  $^{101}\text{Zr}$  [39] and of  $^{107}\text{Mo}$  [40], and, the 1221.2 keV,  $2^+ \rightarrow 0^+$  transition of  $^{130}\text{Sn}$  [41] could not be separated reliably from the 1223.0 keV,  $2^+ \rightarrow 0^+$  transition of  $^{98}\text{Zr}$  [21]. On the contrary, due to the energy resolution for the planar detectors being  $\sim 1$  keV (FWHM) at low  $\gamma$  ray energies [11], the 350.7 keV,  $4^+ \rightarrow 2^+$  transition of  $^{106}\text{Mo}$  was reliably separated in the spectra from three other  $\gamma$  rays, the 352.0 keV,  $(3/2)^+ \rightarrow 1/2^+$  transition of  $^{95}\text{Sr}$  [42], the 352.0 keV,  $(4^+) \rightarrow 2^+$  transition of  $^{100}\text{Zr}$  [22], and the 352.6 keV,  $6^+ \rightarrow 4^+$  transition of  $^{136}\text{Te}$  [43], although the latter three transitions were not separable. The  $2^+ \rightarrow 0^+$  transitions of  $^{104,106}\text{Mo}$  are most likely also contaminated by known [21, 44–48] yrast transitions of  $^{95}\text{Rb}$ ,  $^{99}\text{Sr}$ ,  $^{98}\text{Y}$ ,  $^{103}\text{Zr}$ ,  $^{103,105}\text{Mo}$ , and  $^{145}\text{La}$ , but are included in Table I due to the importance of the Mo fragments in the discussion below. In the case of  $^{132}\text{Sn}$  [27] the  $2^+ \rightarrow 0^+$  transition is a 4041 keV  $\gamma$  ray lying beyond the detection limits of the present experiment due to low efficiency.

The uncertainties for the cross sections reported in Table I are statistical. All cross sections reported in Table I are obtained from the detection of prompt  $\gamma$  rays. Correcting for the possible presence of isomers (half-lives greater than a few nanoseconds) in any of the isotopes studied was not possible from the present data. From the isotopes in Table I, isomers are known in  $^{128}\text{Sn}$ , which has a  $(10^+)$ , 2.91  $\mu\text{s}$  isomer, at 2491.9 keV excitation energy [26], in  $^{132}\text{Sn}$ , which has an  $(8^+)$ , 2.03  $\mu\text{s}$  isomer, at 4848.5 keV excitation energy [27], and in  $^{134}\text{Te}$ , which has a  $(12^+)$ , 18 ns isomer, at 5804.0 keV excitation energy [28]. The presence of the isomers results in an overestimation of the cross section at lower neutron energies ( $E_n = 1.5\text{-}2.0\text{-MeV}$ -bin included) due to the augmentation of the recorded time of flight between the pulsed beam pick-off and the detection of the  $\gamma$  rays emitted from the isomer that is used to determine the inducing neutron energy, and an underestimation of the cross section at higher neutron energies. For instance, considering the case of an  $E_n = 10$  MeV neutron (which has a higher probability to induce fission than an  $E_n = 1.75$  MeV neutron),

it reaches the target at  $\sim 400$  ns after beam pick-off and, assuming that the induced fission populates the 2030 ns isomer in  $^{132}\text{Sn}$ , all such events in which this isomer actually decays  $\sim 570$ -730 ns after population will be recorded in the  $E_n = 1.5$ -2.0 MeV neutron-energy bin. Hence, the yield values deduced in Table I for  $^{128,132}\text{Sn}$  and  $^{134}\text{Te}$  should be deemed as upper limits. The percentage of overestimation depends on the amount of feeding that bypasses the isomers and also on the half-life of the isomer (for half-lives greater than  $1.8 \mu\text{s}$  some decay is lost due to time overlap of sequential micropulses) and can not be estimated experimentally in the present work.

#### IV. DISCUSSION

From the cross sections in Table I one can deduce relative fission fragment yields for the Kr, Sr, Zr, Mo, Sn, Te, Xe, Ba, and Ce fragments. The most reliable relative yields can be obtained from the cross sections for the  $2^+ \rightarrow 0^+$  transitions, however, in cases where the cross sections for the  $2^+ \rightarrow 0^+$  transitions were not determined experimentally, due to contamination of the  $\gamma$ -ray peaks in the spectra or due to low detection efficiency, the cross sections obtained for transitions emitted from higher-spin levels can be used, if they can be corrected for the relative intensity of these transitions as established in previous experiments, assuming, as an approximation, similar level populations. In all such cases in Table I the relative intensities reported for these transitions in  $^{248}\text{Cm}$  and  $^{252}\text{Cf}$  spontaneous-fission experiments were used, except in the case of  $^{132}\text{Sn}$  where the correction was based on the relative intensity reported for the 299.6 keV transition in  $\beta$ -decay [27] due to lack of intensities established in spontaneous-fission experiments. For instance, 75% and 74% relative intensities are reported for the 368.4- and 350.7-keV transitions of  $^{104}\text{Mo}$  and  $^{106}\text{Mo}$ , respectively, in the spontaneous fission of  $^{248}\text{Cm}$  [49].

The yields in Table I can then be compared to the results presented in Fig. 3 of Ref. [10]. For example, from the yields in Table I for  $^{96}\text{Sr}$  and  $^{102}\text{Zr}$ , a  $\sim 1.2$   $^{102}\text{Zr}/^{96}\text{Sr}$  relative yield can be estimated, and from the experimental data in Fig. 3 of Ref. [10] a  $\sim 1.4$  ratio can be deduced, while the prediction from the JEFF-3.1.1 evaluated data library estimate it at  $\sim 1$ , in reasonable agreement with both experimental results. However, huge yield discrepancies are observed for the Mo/Sn isotope pair in Fig. 3 of Ref. [10] between experimental results and evaluated predictions, but the ratios deduced from the yields in Table I are smaller.

For instance, a  $\sim 7$  relative yield for  $^{102}\text{Zr}/^{106}\text{Mo}$  can be estimated from the present data. The same relative yield from the experimental points in Fig. 3 of Ref. [10] is  $\sim 20$ . An overestimation of the predicted yields could still be the case, however, not to the level of 500-600%, as reported in Ref. [10]. We note here that the fission-fragment Mo/Sn yields obtained using X-ray spectroscopy in Ref. [9] in a 0.7-6.0 MeV incident-neutron-energy interval are also more intense compared to the yields in Ref. [10]. The latter also disagree with evaluated fission-fragment yields for a fission neutron spectrum from Refs. [35, 50] and the predictions by the GEF code [51] plotted for comparison as solid and dotted lines in Fig. 2. For completeness, the predictions of the Wahl systematics (CYFP parametrization [52, 53]) is also included in Fig. 2.

The yield obtained in the present work for  $^{104}\text{Mo}$  agrees within uncertainties with the yield reported in Ref. [10]. However, a big difference is observed in Fig. 2 between the corresponding values for  $^{106}\text{Mo}$ . As a result, the fit of the yields for the Mo isotopes in Table I shown in Fig. 2 has an average mass for Mo fragments at  $A=105$ . This is one neutron more than the corresponding fit in Fig. 3 of Ref. [10] and, hence, it brings this value closer to the predictions and the evaluations for the Mo fragments shown in Fig. 4 of Ref. [10]. The GEF yield predictions for the Mo isotopes in Fig. 2 are  $\sim 120\%$  larger than the fit and the results of the CYFP parametrization [52, 53] for the Mo isotopes are  $\sim 10\%$  larger, on average. Hence, for the Mo fragments, the present results are much closer to the Wahl systematics from Refs. [52, 53].

The present experiment and that of Ref. [10] are based on the identification of fragments from detection of the  $\gamma$  rays they emit. The planar detectors of the GEANIE array [11] used in the present experiment exhibit, generally, better energy resolution compared to the detectors in the MINIBALL array [54] used in Ref. [10], but the present experiment had a much lower overall  $\gamma$ -ray efficiency. Only  $\gamma$  rays that exhibit excitation functions similar in shape to the  $^{238}\text{U}(n, f)$  cross section were trusted in the present analysis as being emitted from fission fragments, i.e., the shape of the measured excitation functions qualitatively indicates the fission origin of the  $\gamma$  rays and serves as a means to exclude a  $\gamma$  ray from the analysis if significant contributions from other reactions are present. Moreover, all emitted  $\gamma$  rays, in single and higher-fold events, were recorded. On the other hand, in Ref. [10] only triple and higher-fold  $\gamma$ -ray events were recorded in order to keep the data acquisition rate at a manageable level. Such a condition can negatively affect the detection of low multiplicity



events. For instance, the yield obtained for  $^{132}\text{Sn}$  in Ref. [10] could be affected negatively by the lower number of  $\gamma$  rays emitted, since essentially all  $\gamma$ -ray decay paths have to proceed through the very high excitation energy 4041 keV,  $2^+$  state.

In order to connect the fission product yields to the  $\gamma$ -ray intensity certain assumptions must be made about the amount of side-feeding and the impact of detector effects, such as a  $\gamma$ -ray multiplicity cut. The **CGMF** code, documented in Ref. [55], was used here to determine the impact of these assumptions. **CGMF** is a Monte Carlo implementation of the statistical Hauser-Feshbach decay theory, which determines the prompt neutron and  $\gamma$ -ray emissions from the initial excited fission fragments. It has been used to reproduce many fission observables with reasonable accuracy [56–58]. To begin a **CGMF** calculation one needs the initial distribution of the pre-neutron fragment yields  $Y(A, Z, \text{TKE}, J^\pi)$ , for a fragment mass  $A$ , charge  $Z$ , total kinetic energy TKE, and spin-parity  $J^\pi$ . In the present calculation the fragment mass yields are taken from Ref. [59], the charge distributions are from Wahl systematics [53], the  $\langle \text{TKE} \rangle(A)$  is from Ref. [60], and the spin distribution follows a Gaussian form:

$$P(J|A, Z) \propto (2J + 1) \exp \left[ \frac{-J(J + 1)\hbar^2}{2\alpha T \mathcal{I}_0(A, Z)} \right],$$

where,  $\alpha$  is a spin-scaling factor used to vary the average spin of the fragments  $\langle J \rangle$ ,  $T$  is a nuclear temperature determined from the excitation energy and level density parameter, and  $\mathcal{I}_0(A, Z)$  is the moment of inertia for a rigid rotor of the ground-state shape of a fragment with a particular mass and charge. The parity distribution is assumed to be equal probability for positive and negative parities, i.e.,  $P(J^\pi|A, Z) = \frac{1}{2}P(J|A, Z)$ .

We first sample from the initial fragment distribution  $Y(A, Z, \text{TKE}, J^\pi)$  and then calculate the probability  $P(E_n)$  to emit a neutron with energy  $E_n$  or the probability  $P(E_\gamma)$  to emit a  $\gamma$  ray with energy  $E_\gamma$ . We sample from these probabilities to determine the emission and then repeat this procedure for the new nuclear state until the ground-state or a long-lived isomer is reached. The result is a list of all prompt particles and their energies for each simulated fission event. A global optical potential [61] and the strength-function formalism [62], with parameter values from the 2015-update of RIPL-3 [63], were used to determine the neutron and  $\gamma$ -ray transmission coefficients, respectively. Discrete levels and branching ratios are also from the 2015-update of RIPL-3, and the continuum level densities

are calculated in the Gilbert-Cameron formalism [64].

The CGMF calculations were performed at  $E_n = 1.7$  MeV and  $E_n = 1.8$  MeV and the results were averaged to account for the spread in incident neutron energies. Three spin cases, corresponding to average fragment spins of  $\langle J \rangle = 8.2, 9.9, 11.8 \hbar$  were calculated to span a reasonable range of both  $\langle J \rangle$  and the total prompt  $\gamma$ -ray multiplicity;  $\overline{M}_\gamma = 7.4, 8.4, 9.5 \gamma/\text{fission}$  with no energy threshold and a timing window of 150 ns. Calculations were also performed for three different time coincidence windows of 15 ns, 150 ns, and 1.2  $\mu\text{s}$ . This range in  $\langle J \rangle$  and the timing window were used to investigate the impact of these parameters on the side-feeding and detector effects.

A common assumption found in the literature is that the bulk of the fission events producing a particular fission product will include emission of one or more of their characteristic  $\gamma$  rays, e.g., for even- $Z$  even- $A$  nuclei usually the  $4^+ \rightarrow 2^+$  and the  $2^+ \rightarrow 0^+$  transitions. This can be tested directly in the CGMF calculations and corrections  $\epsilon_L$  can be determined for each transition. Most even- $Z$  even- $A$   $\gamma$ -ray transitions in Table I have  $\epsilon_L$  values between 0.7 and 0.9, indicating that 10 – 30% of the fission product yield could be missed if a characteristic  $\gamma$  ray is not produced. The  $^{128,132}\text{Sn}$  nuclei had  $\epsilon_L < 0.4$ , which represents a significant correction to the default assumption. The calculated  $\epsilon_L$  values varied by 5 – 20% in the explored  $\langle J \rangle$  range. Moreover, the  $\epsilon_L$  values for  $^{128,132}\text{Sn}$  and  $^{134}\text{Te}$  depended on the timing window due to long-lived isomers.

Another correction is due to the energy resolution  $\delta E$  of the  $\gamma$ -ray detectors. Assuming a resolution similar to that in Fig. 12.10 of Ref. [65], a “purity” correction  $\epsilon_P$  can be calculated by selecting the fission events that produce a set of  $\gamma$  rays. Then, the percentage of events in that subset actually emitted by the fission product of interest is  $\epsilon_P$ . Effectively,  $\epsilon_P$  measures the overlap of  $\gamma$  rays within a  $\gamma$ -ray energy range. This correction was found to be very stable with respect to  $\langle J \rangle$  and the timing window. Values of  $\epsilon_P$  varied from 0.10 to 0.90, with most transitions falling in the range 0.70 – 0.85, and are very dependent on the choice of detector resolution.

We also investigated the impact of placing a  $\gamma$ -ray multiplicity cut during the collection of data, as was done in Ref. [10], and also double-gating on transitions to infer yields [66]. This is shown in Fig. 3, where we compare a single-gate method ( $2^+ \rightarrow 0^+$  gate) with a double-gate method ( $4^+ \rightarrow 2^+$  and  $2^+ \rightarrow 0^+$  gate) and show the impact of the level and purity corrections. The calculated yields (lines) use a timing window of 150 ns and average

over all three  $\langle J \rangle$  values. The single-gate (dotted) is determined from the percentage of CGMF fission events “emitting” the  $\gamma$  rays in Table I within the energy-resolution  $\delta E(E_\gamma)$ . The double-gate curve (dashed) require both the  $4^+ \rightarrow 2^+$  and  $2^+ \rightarrow 0^+$  transitions for the specified fission product. The double-gate lowers most of the inferred yields, but the  $^{128,132}\text{Sn}$  nuclei are more dramatically affected because they have large level spacings and are often not produced with enough excitation energy to emit both the  $4^+ \rightarrow 2^+$  and  $2^+ \rightarrow 0^+$  transitions. The inferred yields for  $^{106}\text{Mo}$  and  $^{128,132}\text{Sn}$  in Ref. [10] show a similar decrease for these nuclei while the value obtained in the present work for  $^{106}\text{Mo}$  is not as dramatically affected. While the primary purpose of Fig. 3 is to illustrate the impact of using a single-gate or double-gate on the inferred yield, it is worth noting here that the corrected CGMF yields (solid line) show better agreement with data and the evaluated values of England & Rider [50] than the uncorrected yields.

We have also investigated the impact of a multiplicity cut on the inferred yields. Our calculations reveal that a total  $\gamma$ -ray multiplicity cut affects more the Mo and Sn isotopes, as shown in Table II. For a total  $\gamma$ -ray multiplicity cut of  $\overline{M}_\gamma^T \geq 9$ , the inferred yield of the Mo and Sn isotopes are reduced by about 25% more than all other studied isotopes. Similar results were found when we considered a single-gate as well. Overall, the present theoretical analysis of experimental results suggests that a significant portion of the yield discrepancies may be caused by the use of  $\gamma$ -ray multiplicity cuts and inferring the yields via double-gating.

## V. SUMMARY

Fast neutrons from the LANSCE/WNR facility induced fission on  $^{238}\text{U}$  to obtain information on the prompt  $\gamma$ -ray yield of the produced even-even fission fragments. The significant yield discrepancies (500-600%) reported recently [10] between experimental results and predictions/evaluations for the Mo/Sn pair in fast-neutron induced reactions on  $^{238}\text{U}$  using  $\gamma$ - $\gamma$ - $\gamma$  coincidence spectroscopy were addressed. Our singles  $\gamma$ -ray results give better agreement. A theoretical analysis using the CGMF code highlights the portion of the discrepancies that can be caused by the use of  $\gamma$ -ray multiplicity cuts and inferring yields by gating on characteristic  $\gamma$  rays.

## ACKNOWLEDGMENTS

This work was performed under the auspices of the U.S. Department of Energy (DOE) under Contract No. DE-AC52-06NA25396. This work has benefitted from use of the LAN-SCE accelerator facility supported under DOE Contract No. DE-AC52-06NA25396. This work was in part supported by the Office of Defense Nuclear Nonproliferation Research & Development, National Nuclear Security Administration, U.S. DOE. We thank J. N. Wilson for sharing their experimental results reported in Fig. 3 of Ref. [10].

- 
- [1] J. B. Wilhelmy, E. Cheifetz, R. C. Jared, S. G. Thompson, H. R. Bowman, and J. O. Rasmussen, *Phys. Rev. C* **5**, 2041 (1972).
  - [2] I. Ahmad and W. R. Phillips, *Rep. Prog. Phys.* **58**, 1415 (1995).
  - [3] J. H. Hamilton *et al.*, *Prog. Part. in Nucl. Phys.* **35**, 635 (1995).
  - [4] N. Fotiades *et al.*, *Physica Scripta Vol. T88*, 127 (2000).
  - [5] A. Bogachev *et al.*, *Eur. Phys. J. A* **34**, 23 (2007).
  - [6] W. R. Phillips *et al.*, *Eur. Phys. J. A* **3**, 205 (1998).
  - [7] S. Nagy *et al.*, *Phys. Rev. C* **17**, 163 (1978).
  - [8] J. Laurec *et al.*, *Nucl. Data Sheets* **111**, 2965 (2010).
  - [9] T. Granier *et al.*, *Eur. Phys. J. A* **49**, 114 (2013).
  - [10] J. N. Wilson *et al.*, *Phys. Rev. Lett.* **118**, 222501 (2017).
  - [11] J. A. Becker and R. O. Nelson, *Nucl. Phys. News International* **7**, 11 (1997).
  - [12] P. W. Lisowski, C. D. Bowman, G. J. Russell, and S. A. Wender, *Nucl. Sci. Eng.* **106**, 208 (1990).
  - [13] P. W. Lisowski and K. F. Schoenberg, *Nucl. Instrum. Methods Phys. Res., Sect. A* **562**, 910 (2006).
  - [14] S. P. Simakov, A. Pavlik, H. Vonach, and S. Hlaváč, *INDC(CCP)-413* (1998).
  - [15] N. Fotiades *et al.*, *Phys. Rev. C* **69**, 024601 (2004).
  - [16] T. Ethvignot *et al.*, *J. Nucl. Sci. Technol. Supplement* **2**, 254 (2002).
  - [17] T. Ethvignot in *Fission product yield data for the transmutation of minor actinide nuclear waste. International Atomic Energy Agency*, ISBN 92-0-115306-6, p. 16 (2008).

- [18] P. Casoli, Etude de la production de fragments dans la fission induite par neutrons sur l'uranium-238, Ph.D. thesis, Université de Bordeaux (2003).
- [19] C. M. Baglin, Nucl. Data Sheets **113**, 2187 (2012).
- [20] D. Abriola and A. A. Sonzogni, Nucl. Data Sheets **109**, 2501 (2008).
- [21] B. Singh and Z. Hu, Nucl. Data Sheets **98**, 335 (2003).
- [22] B. Singh, Nucl. Data Sheets **109**, 297 (2008).
- [23] D. De Frenne, Nucl. Data Sheets **110**, 1745 (2009).
- [24] J. Blachot, Nucl. Data Sheets **108**, 2035 (2007).
- [25] D. De Frenne and A. Negret, Nucl. Data Sheets **109**, 943 (2008).
- [26] Z. Elekes and J. Timar, Nucl. Data Sheets **129**, 191 (2015).
- [27] Yu. Khazov, A. A. Rodionov, S. Sakharov, and B. Singh, Nucl. Data Sheets **104**, 497 (2005).
- [28] A. A. Sonzogni, Nucl. Data Sheets **103**, 1 (2004).
- [29] A. A. Sonzogni, Nucl. Data Sheets **98**, 515 (2003).
- [30] N. Nica, Nucl. Data Sheets **108**, 1287 (2007).
- [31] A. A. Sonzogni, Nucl. Data Sheets **93**, 599 (2001).
- [32] Yu. Khazov, A. Rodionov, and G. Shulyak, Nucl. Data Sheets **136**, 163 (2016).
- [33] N. Nica, Nucl. Data Sheets **117**, 1 (2014).
- [34] S. K. Basu and A. A. Sonzogni, Nucl. Data Sheets **114**, 435 (2013).
- [35] M. B. Chadwick *et al.*, Nucl. Data Sheets **112**, 2887 (2011).
- [36] P E Garrett *et al.*, Phys. Rev. C **68**, 024312 (2003).
- [37] N Fotiades *et al.*, Phys. Rev. C **75** 054322 (2007).
- [38] N. Fotiades *et al.*, Phys. Rev. C **84**, 054310 (2011).
- [39] J. Blachot, Nucl. Data Sheets **83**, 1 (1998).
- [40] J. Blachot, Nucl. Data Sheets **109**, 1383 (2008).
- [41] B. Singh, Nucl. Data Sheets **93**, 33 (2001).
- [42] S. K. Basu, G. Mukherjee, and A. A. Sonzogni, Nucl. Data Sheets **111**, 2555 (2010).
- [43] A. A. Sonzogni, Nucl. Data Sheets **95**, 837 (2002).
- [44] G. S. Simpson *et al.*, Phys. Rev. C **82**, 024302 (2010).
- [45] E. Browne and J. K. Tuli, Nucl. Data Sheets **145**, 25 (2017).
- [46] D. De Frenne, Nucl. Data Sheets **110**, 2081 (2009).
- [47] D. De Frenne and E. Jacobs, Nucl. Data Sheets **105**, 775 (2005).

- [48] E. Browne and J. K. Tuli, Nucl. Data Sheets **110**, 507 (2009).
- [49] M. A. C. Hotchkiset *al.*, Nucl. Phys. **A530**, 111 (1991).
- [50] T. R. England and B. F. Rider, Los Alamos National Laboratory Report LA-UR-94-3106, (1994).
- [51] K.-H. Schmidt, B. Jurado, C. Amouroux, and C. Schmitt, Nucl. Data Sheets **131**, 107 (2016).
- [52] A. C. Wahl, IAEA-TECDOC-1168, p. 58, (2000).
- [53] A. C. Wahl, Los Alamos National Laboratory Report LA-13928, (2002).
- [54] N. Warr *et al.*, Eur. Phys. J. A **49**, 40 (2013).
- [55] B. Becker, P. Talou, T. Kawano, Y. Danon, and I. Stetcu, Phys. Rev. C **87**, 014617 (2013).
- [56] I. Stetcu, P. Talou, T. Kawano, and M. Jandel, Phys. Rev. C **88**, 044603 (2013).
- [57] I. Stetcu, P. Talou, T. Kawano, and M. Jandel, Phys. Rev. C **90**, 024617 (2014).
- [58] P. Talou, T. Kawano, I. Stetcu, J. P. Lestone, E. McKigney, and M. B. Chadwick, Phys. Rev. C **94**, 064613 (2016).
- [59] F. Vivès, F.-J. Hamsch, H. Bax, and S. Oberstedt, Nucl. Phys. **A662**, 63 (2000).
- [60] E. Birgersson, A. Oberstedt, S. Oberstedt, and F.-J. Hamsch, Nucl. Phys. **A817**, 1 (2009).
- [61] A. Koning and J. Delaroche, Nucl. Phys. **A713**, 231 (2003).
- [62] J. Kopecky and M. Uhl, Phys. Rev. C **41**, 1941 (1990).
- [63] R. Capote *et al.*, Nucl. Data Sheets **110**, 3107 (2009).
- [64] A. Gilbert and A. G. W. Cameron, Canadian Journal of Physics, **43**, 1446 (1965).
- [65] G. F. Knoll, *Radiation detection and measurement* (John Wiley & Sons, 2010).
- [66] J. N. Wilson, private communication, (2018).

TABLE I. Partial  $\gamma$ -ray cross sections for previously known transitions [19–34] of Kr, Sr, Zr, Mo, Sn, Te, Xe, Ba, and Ce fragments at  $E_n \sim 1.75$  MeV determined in the present experiment and deduced isotopic yields.

Isotope	Transition Energy (keV)	Cross section (mb)	$J_i^\pi \rightarrow J_f^\pi$	Yield (mb)
$^{92}\text{Kr}$	769.2	10.0(8)	$2^+ \rightarrow 0^+$	10.0(8)
$^{96}\text{Sr}$	815.0	13.7(9)	$2^+ \rightarrow 0^+$	13.7(9)
$^{98}\text{Sr}$	289.3	6.3(5)	$4^+ \rightarrow 2^+$	8.2(7)
$^{100}\text{Zr}$	497.1	9.9(5)	$(6^+) \rightarrow (4^+)$	15.2(8)
$^{102}\text{Zr}$	151.8	19.0(7)*	$2^+ \rightarrow 0^+$	<19.7
	326.5	11.2(6)	$4^+ \rightarrow 2^+$	16.2(9)
$^{104}\text{Zr}$	312.2	3.1(4)	$(4^+) \rightarrow (2^+)$	3.3(5)
$^{104}\text{Mo}$	192.2	10.1(4)*	$2^+ \rightarrow 0^+$	<10.5
	368.4	2.2(4)	$4^+ \rightarrow 2^+$	2.9(6)
$^{106}\text{Mo}$	171.6	10.5(4)*	$2^+ \rightarrow 0^+$	<10.9
	350.7	1.8(4)	$4^+ \rightarrow 2^+$	2.4(6)
$^{128}\text{Sn}$	1168.8	2.5(4)	$(2)^+ \rightarrow 0^+$	<2.9
$^{132}\text{Sn}$	299.6	4.0(4)	$(6^+) \rightarrow (4^+)$	<5.5
$^{134}\text{Te}$	1279.0	24.5(3)	$2^+ \rightarrow 0^+$	<24.8
	297.0	20.8(8)	$4^+ \rightarrow 2^+$	
$^{138}\text{Te}$	443.1	4.6(8)	$(2^+) \rightarrow 0^+$	4.6(8)
$^{138}\text{Xe}$	588.8	9.6(8)	$2^+ \rightarrow 0^+$	9.6(8)
$^{140}\text{Xe}$	376.7	16.6(9)	$2^+ \rightarrow 0^+$	16.6(9)
	457.6	12.5(7)	$4^+ \rightarrow 2^+$	
$^{144}\text{Ba}$	330.9	9.2(7)	$4^+ \rightarrow 2^+$	9.7(7)
$^{146}\text{Ba}$	332.4	7.1(6)	$4^+ \rightarrow 2^+$	7.9(7)
$^{148}\text{Ba}$	281.3	1.3(3)	$4^+ \rightarrow 2^+$	1.5(4)
$^{150}\text{Ce}$	208.7	3.0(5)	$4^+ \rightarrow 2^+$	4.2(7)

\*Includes strength by more than one transition of more than one fission fragments.



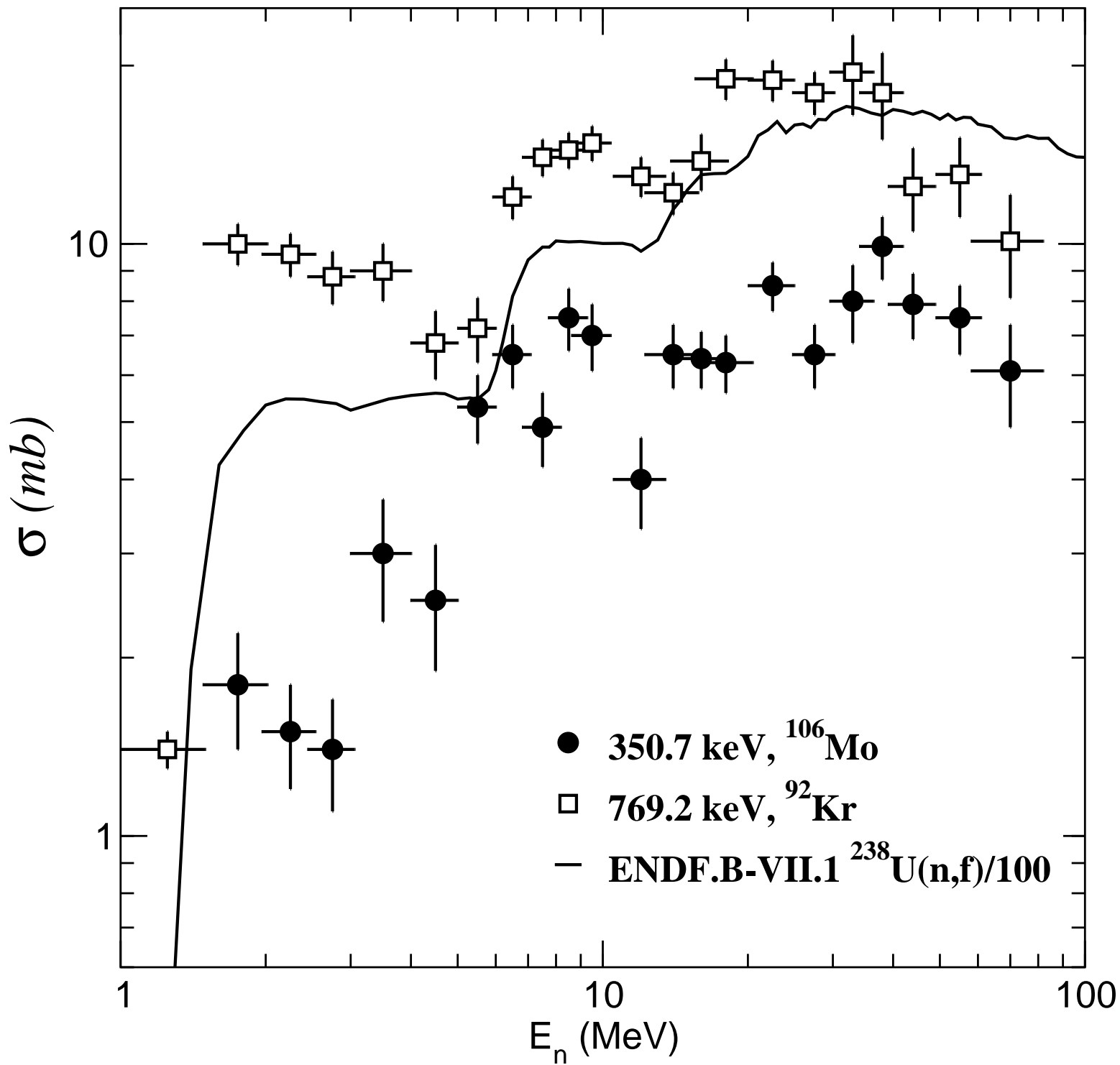
TABLE II. Ratio of the inferred yield using a double-gate on the  $4^+ \rightarrow 2^+$  and  $2^+ \rightarrow 0^+$  transitions with a given total  $\gamma$ -ray multiplicity  $\overline{M}_\gamma^T$  cut and without.

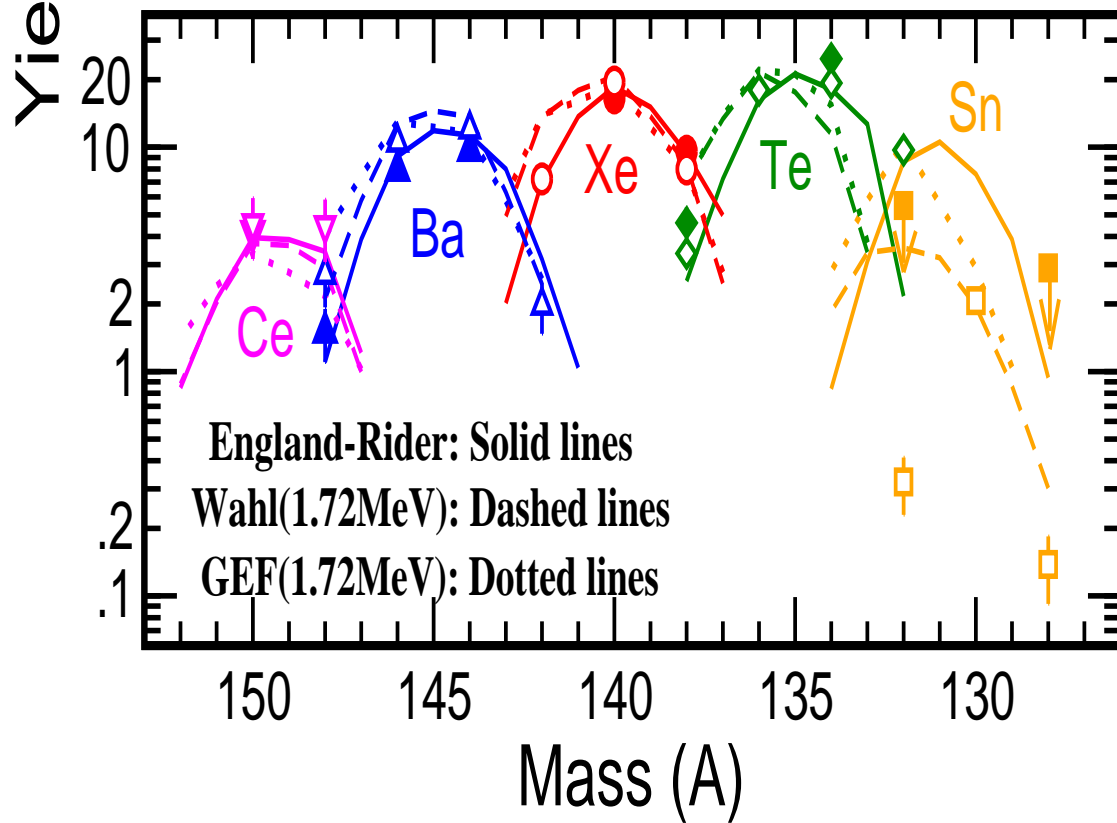
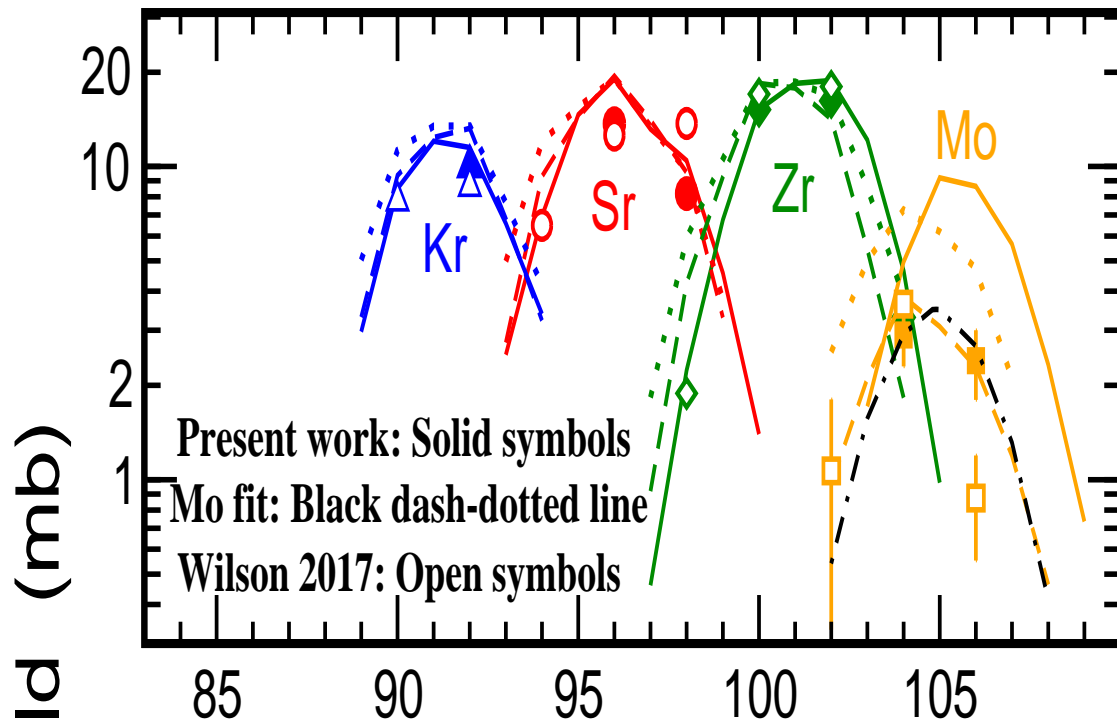
Total Multiplicity Cut	$^{104,106}\text{Mo}$ and $^{128,132}\text{Sn}$	All others
$\overline{M}_\gamma^T \geq 3$	0.993	0.996
$\overline{M}_\gamma^T \geq 6$	0.829	0.898
$\overline{M}_\gamma^T \geq 9$	0.422	0.620

FIG. 1. Cross section values as a function of incident neutron energy obtained for the 350.7-keV (solid circles) and the 769.2-keV (open squares) transitions of  $^{106}\text{Mo}$  and of  $^{92}\text{Kr}$ , respectively, in the present work. The solid line is the total  $^{238}\text{U}(n, f)$  cross section from Ref. [35] divided (arbitrarily) by a factor of 100.

FIG. 2. (Color online) Yields from Table I (solid symbols) plotted versus mass of the fragments. The yield values for  $^{128,132}\text{Sn}$  and  $^{134}\text{Te}$  are upper limits due to known isomers (see text). The black dash-dotted line is a Gaussian fit to the yields obtained for  $^{104}\text{Mo}$  and  $^{106}\text{Mo}$  in the present work. The experimental yields from Fig. 3 of Ref. [10], multiplied by the  $^{238}\text{U}(n, f)$ , 460 mb [35] cross section at  $E_n = 1.72$  MeV, are included as open symbols. The solid lines are the evaluated product yields for a fission neutron spectrum as quoted in Ref. [50], the dashed lines are the Wahl systematics (CYFP parametrization) [52, 53] at  $E_n = 1.72$  MeV, and the dotted lines are the predictions by the GEF code [51] at  $E_n = 1.72$  MeV, all normalized by multiplication by 460 mb.

FIG. 3. (Color online) Inferred fission product yield for 18 even- $Z$  even- $A$  nuclei determined from  $\gamma$ -ray spectroscopy. The yields are calculated either using a single  $\gamma$ -ray transition (dotted) or a double-gate on the  $4^+ \rightarrow 2^+$  and  $2^+ \rightarrow 0^+$  transitions (dashed). The solid line indicates single-gate yields that have been corrected with the level  $\epsilon_L$  and purity  $\epsilon_P$  corrections (see text). Also shown are the GEANIE yields obtained in the present work from Table I, those determined in Ref. [10] (Wilson, 2017), and interpolated values from the evaluation in Ref. [50] (England & Rider).





<sup>96</sup>Sr <sup>100</sup>Zr <sup>104</sup>Zr <sup>106</sup>Mo <sup>132</sup>Sn <sup>138</sup>Te <sup>140</sup>Xe <sup>146</sup>Ba <sup>150</sup>Ce

Independent Yield (%/fission)

